MLL3/4 methyltransferases regulate the differentiation of pluripotent stem cells through coordinating glycolysis and mitochondrial respiration

Suza Mohammad Nur[1,3], Yunbo Jia[1], Muyi Ye[1], Caylin A. Lepak[1], Issam Ben-Sahra[4,5], and Kaixiang Cao[1,2,3,*]

[1]Department of Biochemistry, Case Western Reserve University

[2]Department of Genetics and Genome Sciences, Case Western Reserve University

[3]Case Comprehensive Cancer Center, Case Western Reserve University, Cleveland, OH 44106, USA

[4]Department of Biochemistry and Molecular Genetics, Northwestern University

[5]Robert H. Lurie Comprehensive Cancer Center, Northwestern University, Chicago, IL 60611, USA

Running title: MLL3/4 regulate cellular respiration to facilitate pluripotent stem cell differentiation

Keywords: MLL3, MLL4, stem cells, differentiation, cellular metabolism, glycolysis, TCA cycle

*Correspondence should be sent to the following address:

Kaixiang Cao, PhD

Department of Biochemistry, School of Medicine, Case Western Reserve University

10900 Euclid Avenue, Cleveland, OH 44106, USA

Office: (216) 368-1218

Email: kxc725@case.edu

Abstract

Enhancer-regulating epigenetic modifiers play critical roles in normal physiological processes and human pathogenesis. The major enhancer regulator paralogs MLL3 and MLL4 (MLL3/4) belong to the lysine methyltransferase 2 (KMT2) family, which catalyzes the methylation of lysine 4 on histone H3 (H3K4me). MLL3/4 are required for enhancer activation and are essential for mammalian development and stem cell differentiation. Although recent studies have linked MLL3/4 with different metabolic pathways in the regulation of stem cell self-renewal and cancer cell growth, the mechanisms connecting enhancer function to metabolic control remain elusive. Here, using respiration flux assays, stable isotope tracing, transcriptomics, and stem cell biology techniques, we show that the loss of MLL3/4 impairs glycolysis and mitochondrial respiration in murine embryonic stem cells. Mechanistically, MLL3/4 deficiency suppresses the expression of the rate-limiting glycolytic enzyme hexokinase 2 (HK2) and compromises the function of the oxoglutarate dehydrogenase (OGDH) complex, thereby coordinately impairing central carbon metabolism. Remarkably, combined restoration of HK2 and OGDH rescues the metabolic defects caused by MLL3/4 loss and reinstates differentiation capacity. Taken together, our study identifies a direct link between enhancer-regulating epigenetic machineries and metabolic control of cell fate transition, providing a mechanistic framework for understanding how enhancer malfunction contributes to developmental abnormalities and human diseases.

Introduction

Enhancer deregulation is a major driver of human congenital disorders (*1-4*). In mammals, nucleosomes at enhancers are mono-methylated on lysine 4 of histone H3 (H3K4) by the paralogous enzymes Mixed-lineage Leukemia 3 (MLL3, also known as KMT2C) and Mixed-lineage Leukemia 4 (MLL4, also known as KMT2D) (*5-9*). Mice null for MLL4 die shortly after gastrulation, while MLL3 loss leads to neonatal lethality (*10, 11*). Heterozygous loss-of-function mutations in MLL4 lead to Kabuki syndrome (*1*) and those in MLL3 cause Kleefstra syndrome 2 (*4, 12, 13*). Both disorders are characterized by craniofacial dysmorphism and developmental delay, highlighting the instructive role of MLL3/4 in normal development and human pathogenesis. However, molecular mechanisms by which MLL3/4 function in biologically normal and pathological processes remain poorly understood.

Recent results have revealed a functional link between MLL3/4 and cellular metabolism. MLL3/4 and nucleotide synthesis pathways co-regulate the self-renewal of pluripotent stem cells (PSCs) (*14*). Moreover, steady-state abundance of glycolytic metabolites such as glucose-6-phosphate (G6P) and fructose-6-phosphate (F6P), and tricarboxylic acid (TCA) cycle metabolites including succinate, fumarate, and malate, is reduced in PSCs lacking MLL3/4 (*14*). In contrast, MLL4-deficient lung cancer and melanoma cells adopt upregulated glycolysis (*15, 16*), suggesting a context-dependent role of MLL3/4 in regulating cellular metabolism. How MLL3/4 modulate metabolic pathways and whether they govern cell fate via these pathways are largely unknown.

Glycolysis and mitochondrial respiration are tightly regulated in PSCs. Naive PSCs, such as murine embryonic stem cells (ESCs), exhibit metabolic bivalency, utilizing both glycolysis and mitochondrial respiration for energy production, whereas primed PSCs are predominantly glycolytic (*17*). On the other hand, somatic cells are more dependent on mitochondrial respiration

66 (*18, 19*). Inhibition of glycolysis drives the exit from pluripotency, while stimulation of glycolysis
67 enhances somatic cell reprogramming to induced PSCs (iPSCs) (*18, 20*), suggesting that the
68 balance between glycolysis and mitochondrial respiration instructs cell fate transition. To date,
69 how metabolic states are established during development and whether they instruct cell identity
70 remain enigmatic.

71 To investigate the functional relationship of MLL3/4, cellular metabolism, and PSC
72 differentiation, we examined the impact of MLL3/4 loss on glycolysis and mitochondrial
73 respiration in ESCs. Both extracellular acidification rate (ECAR) and oxygen consumption rate
74 (OCR) are reduced in MLL3/4-null ESCs. Stable isotope tracing reveals a reduction in the labeling
75 of specific metabolites in both glycolysis and the TCA cycle upon MLL3/4 loss. MLL3/4 are
76 required for the expression of hexokinase 2 (HK2) and for proper lipoylation of dihydrolipoamide
77 S-succinyltransferase (DLST), the E2 subunit of the oxoglutarate dehydrogenase complex
78 (OGDHc). Moreover, combined overexpression of HK2 and OGDH partially rescues the
79 metabolic and differentiation defects caused by MLL3/4 loss. Our results provide novel insight
80 into understanding the crosstalk between epigenetic machineries and cellular metabolism.
81 Importantly, they may pave the way for developing novel strategies to target human diseases driven
82 by enhancer deregulation.
83

Results

MLL3/4 loss dampens glycolytic activity in ground-state ESCs

We previously found that the loss of MLL3/4 in ESCs reduced the steady-state abundance of glycolytic intermediates, including G6P and F6P (*14*), suggesting that MLL3/4 regulate glycolysis in naive PSCs. To directly test this idea, we measured the ECAR of wildtype (WT) and MLL3/4 double knockout (DKO) ESCs (*14*) using a glycolysis stress assay. MLL3/4 deficiency markedly reduced both basal glycolysis and glycolytic capacity (Fig. 1A-C), suggesting that MLL3/4 are required to maintain the glycolytic activity in naive PSCs. To determine if the decreased steady-state abundance of glycolytic metabolites reflects impaired glucose metabolism, we next performed stable isotope tracing with [$^{13}C_6$]-glucose in WT and MLL3/4 DKO ESCs, followed by liquid chromatography-tandem mass spectrometry (LC-MS/MS) analysis (Fig. 1D). Consistent with results in steady-state metabolomics, the incorporation of ^{13}C into F6P/G1P (glucose-1-phosphate)/G6P (m+6) was significantly reduced by MLL3/4 loss (Fig. 1E and Fig. S1A). Moreover, MLL3/4 loss reduced labeling of lactate (m+3) from [$^{13}C_6$]-glucose (Fig. 1F and Fig. S1B), corresponding to the decreased glycolytic activity in MLL3/4 DKO ESCs. To determine whether this defect was caused by reduced glucose import, we measured glucose uptake and found no significant difference between WT and MLL3/4 DKO ESCs (Fig. 1G). These findings indicate that MLL3/4 loss does not impair glucose entry into cells but instead disrupts early rate-limiting steps in glycolysis, thereby suppressing glycolysis in ESCs.

To elucidate the mechanism underlying this defect, we examined RNA-seq data (*14*) for genes encoding glycolytic enzymes involved in the production and utilization of G6P and F6P. Among these, *Hk2*, which encodes hexokinase 2, the enzyme that catalyzes the first committed step of glycolysis by converting glucose to G6P, was significantly downregulated in MLL3/4 DKO

107 ESCs (Fig. S1C). On the other hand, the expression levels of genes encoding glucose-6-phosphate
108 isomerase (*Gpi1*), phosphofructokinase 1 (*Pfkl* and *Pfkp*), and phosphofructokinase 2 (*Pfkfb1* and
109 *Pfkfb2*) were largely unchanged (Fig. S1C). Consistent with the transcriptomic data, western
110 blotting analysis showed that HK2 protein levels were markedly reduced by MLL3/4 loss, whereas
111 levels of HK1 (hexokinase 1), the paralog of HK2, remained largely unaffected (Fig. 1H). To
112 investigate how MLL3/4 regulate *Hk2* expression, we analyzed ChIP-seq datasets (*7, 14*) and
113 found at least six putative enhancers near the *Hk2* locus, which were bound by MLL4 and exhibited
114 reduced H3K27ac levels in MLL3/4 DKO ESCs (Fig. S1D). These data suggest that MLL3/4 could
115 promote *Hk2* expression through these putative enhancers. Taken together, our results indicate that
116 glycolysis in naive PSCs requires MLL3/4 and that the decreased HK2 levels may be responsible
117 for the defective glycolysis caused by MLL3/4 loss.
118
119 **MLL3/4 are required for mitochondrial respiration in ground-state ESCs**
120 Metabolic bivalency, defined by the concurrent use of glycolysis and mitochondrial respiration, is
121 one of the hallmarks of naive PSCs (*21, 22*). To examine the role of MLL3/4 in regulating
122 mitochondrial respiration in naive PSCs, we measured the OCR of WT and MLL3/4 DKO ESCs
123 using a mitochondrial stress assay. Interestingly, MLL3/4 deficiency significantly reduced both
124 basal and maximal respiration (Fig. 2A-C), suggesting that MLL3/4 are required to maintain the
125 bivalent metabolic program of naive PSCs. To define where mitochondrial metabolism was
126 disrupted, we performed stable isotope tracing with [$^{13}C_6$]-glucose labeling (Fig. 2D). MLL3/4
127 loss did not have a significant impact on the labeling of citrate/isocitrate (m+2) and alpha-
128 ketoglutarate (α-KG; m+2) (Fig. 2E-F and Fig. S2A-B). In contrast, labeling of succinate (m+2),
129 fumarate (m+2), and malate (m+2) was significantly reduced in MLL3/4 DKO ESCs (Fig. 2G-I

130 and Fig. S2C-E). These findings suggest that MLL3/4 loss disrupts TCA cycle activity downstream
131 of α-KG, thereby contributing to the impaired mitochondrial respiration.

132 To further test this model, we traced glutamine carbon entry into the TCA cycle using
133 [$^{13}C_5$]-glutamine (Fig. 2J). Although MLL3/4 loss did not significantly affect labeling of glutamate
134 (m+5) (Fig. 2K and Fig. S2F), that of α-KG (m+5) was significantly reduced in MLL3/4 DKO
135 ESCs (Fig. 2L and Fig. S2G). This reduction may reflect impaired conversion of glutamate to α-
136 KG, although the expression levels of *Glud1*, which encodes glutamate dehydrogenase (GDH), the
137 enzyme catalyzing the conversion of glutamate to α-KG, were comparable between WT and
138 MLL3/4 DKO ESCs (Fig. S2L). Consistent with results from [$^{13}C_6$]-glucose labeling, labeling of
139 succinate (m+4), fumarate (m+4), and malate (m+4) from [$^{13}C_5$]-glutamine was significantly
140 reduced in MLL3/4 DKO ESCs, while that of citrate/isocitrate (m+4) was largely unchanged (Fig.
141 2M-P and Fig. S2H-K). Furthermore, expression levels of multiple genes encoding enzymes
142 involved in α-KG and downstream TCA cycle metabolism were comparable between MLL3/4
143 DKO and WT ESCs (Fig. S2L). In addition, protein levels of OGDH, SUCLA2, SUCLG1,
144 SUCLG2, and SDHA remained largely unperturbed upon MLL3/4 loss (Fig. 2Q and Fig. S2M-N),
145 suggesting that MLL3/4 regulate TCA cycle metabolites via mechanisms other than transcriptional
146 control of metabolic enzymes.

147 To further elucidate the molecular mechanisms by which MLL3/4 regulate the TCA cycle,
148 we examined the protein levels of DLST and dihydrolipoamide dehydrogenase (DLD), E2 and E3
149 components of the OGDHc. MLL3/4 loss had little impact on their levels (Fig. 2R-S), suggesting
150 that MLL3/4 are unlikely to regulate mitochondrial respiration via modulating the abundance of
151 OGDHc components. Lipoylated DLST is essential for OGDHc activity and for the conversion of
152 α-KG to succinyl-CoA (*23-25*). To understand if MLL3/4 loss impairs the activity of DLST, we

153 examined the levels of lipoylated proteins in WT and MLL3/4 DKO ESCs using a specific anti-
154 lipoate antibody (*26*). MLL3/4 loss led to a reproducible decrease of the lipoylated protein species
155 with lower molecular weight, attributed to lipoylated DLST based on its size (Fig. 2T). The
156 decrease in lipoylation was specific to DLST as levels of other abundantly lipoylated proteins in
157 the mitochondria, such as dihydrolipoamide acetyltransferase (DLAT) in the pyruvate
158 dehydrogenase complex and dihydrolipoamide branched-chain transacylase (DBT) in the
159 branched-chain alpha-keto acid dehydrogenase complex (*24, 25*), were comparable in MLL3/4
160 DKO and WT ESCs (Fig. 2T). Taken together, these results suggest that MLL3/4 loss impairs
161 mitochondrial respiration and disrupts metabolic flux through reducing DLST lipoylation in naive
162 PSCs.
163
164 **Combined overexpression of HK2 and OGDH rescues metabolic defects caused by MLL3/4**
165 **loss**
166 To determine if MLL3/4 regulate glycolysis and mitochondrial respiration in ESCs through
167 activating HK2, we overexpressed 3×HA-tagged HK2 in MLL3/4 DKO ESCs with a doxycycline
168 (DOX)-inducible system (*27, 28*) (Fig. S3A). HK2 overexpression increased basal glycolysis and
169 glycolytic capacity in MLL3/4 DKO cells (Fig. S3B-D); however, OCR during basal respiration
170 was reduced upon HK2 expression (Fig. S3E-G), suggesting that HK2 overexpression renders
171 MLL3/4 DKO ESCs more dependent on glycolysis for energy production.
172 Since HK2 overexpression led to an expected increase in ECAR but a reduction in OCR,
173 we sought to restore both glycolysis and mitochondrial respiration in MLL3/4 DKO ESCs to study
174 the functional relationship of MLL3/4, metabolic state, and the differentiation capability of PSCs.
175 We hypothesized that the decrease of ^{13}C incorporation in succinate, fumarate, and malate in both

176 [$^{13}C_6$]-glucose and [$^{13}C_5$]-glutamine labelled MLL3/4-null ESCs results from the defective
177 OGDHc. Although OGDH levels were comparable between MLL3/4 DKO and WT ESCs, OGDH
178 overexpression could potentially compensate for the functionally impaired OGDHc and reduced
179 TCA cycle metabolites in MLL3/4-null ESCs. We therefore overexpressed 3×HA-tagged HK2 and
180 3×FLAG-tagged OGDH together in MLL3/4 DKO ESCs using DOX-inducible expression vectors
181 carrying distinct drug resistance genes (Fig. 3A). Increased levels of HK2 and OGDH led to
182 elevated rates of basal glycolysis, glycolytic capacity, and both basal and maximal respiration (Fig.
183 3B-G). Furthermore, stable isotope tracing by labeling MLL3/4 DKO and HK2/OGDH double-
184 overexpressing (DOE) MLL3/4 DKO cells with [$^{13}C_6$]-glucose indicated that labeling of
185 metabolites reduced by MLL3/4 loss such as F6P/G1P/G6P (m+6), lactate (m+3), succinate (m+2),
186 and fumarate (m+2) was partially restored by HK2/OGDH DOE (Fig. 3H-M, Fig. S4A-B, and Fig.
187 S4E-G). As expected, we did not observe a significant difference in the labeling of citrate/isocitrate
188 (m+2) or α-KG (m+2) (Fig. 3J and Fig. S4C-E). Notably, malate (m+2) labeling was not
189 significantly increased upon HK2/OGDH DOE in MLL3/4 DKO cells (Fig. 3M and Fig. S4H),
190 suggesting that there are additional regulatory layers on the levels of malate besides HK2 and
191 OGDHc. Taken together, these results suggest that MLL3/4 regulate glycolysis and mitochondrial
192 respiration through activating *Hk2* expression and maintaining the normal function of the OGDHc.
193

194 **Combined overexpression of HK2 and OGDH rescues differentiation defects caused by**
195 **MLL3/4 loss**

196 To assess the impact of MLL3/4 loss on cell fate transition, we generated embryoid bodies (EBs)
197 from WT and MLL3/4 DKO ESCs. As expected, MLL3/4 loss led to a decrease in the size of day
198 6 EBs (Fig. 4A-B), indicating that MLL3/4 are required for PSC differentiation. RNA-seq analysis

199 showed that MLL3/4 loss caused the significant deregulation of 4,547 genes in day 6 EBs (Fig.
200 4C). Among genes significantly downregulated in MLL3/4 DKO EBs, 52.3% (1,192 of 2,280)
201 were significantly upregulated during WT EB differentiation (Fig. 4D), suggesting that these genes
202 are dependent on MLL3/4 to be activated during differentiation. We thus defined them as MLL3/4-
203 dependent differentiation genes. Gene ontology (GO) analysis showed that the top 300 upregulated
204 genes of the 1,192 MLL3/4-dependent differentiation genes were enriched with embryogenesis-
205 related genes and known MLL4 targets essential for actin cytoskeleton organization (*7*) (Fig. 4E),
206 further indicating that MLL3/4 loss impairs PSC differentiation. Indeed, pluripotency genes were
207 significantly upregulated in MLL3/4 DKO EBs and marker genes of meso- and endo-derm
208 lineages were downregulated in EBs by MLL3/4 loss (Fig. S5A-B). These data demonstrate that
209 MLL3/4 are required for PSC differentiation and related transcriptional reconfiguration.

210 To examine if the partial restoration of glycolysis and mitochondrial respiration had any
211 impact on the differentiation capacity of ESCs lacking MLL3/4, we treated MLL3/4 DKO and
212 HK2/OGDH DOE MLL3/4 DKO cells with DOX and differentiated them toward EBs. EB
213 differentiation revealed that HK2/OGDH DOE led to a significant increase in the size of day 6
214 EBs (Fig. 4F-G), suggesting that restoring glycolysis and mitochondrial respiration rescues
215 differentiation defects caused by MLL3/4 loss. Moreover, RNA-seq analysis identified 1,778
216 significantly deregulated genes by HK2/OGDH DOE compared with MLL3/4 DKO ESCs treated
217 with DOX (Fig. 4H). Gene set enrichment analysis (GSEA) and hierarchical clustering analysis of
218 MLL3/4-dependent differentiation genes (Fig. 4D) revealed a significant upregulation of them
219 upon HK2/OGDH DOE (Fig. 4I-J). Indeed, 34.3% of genes upregulated by HK2/OGDH DOE
220 (300 of 875) were dependent on MLL3/4 to be activated during differentiation (Fig. 4K),
221 suggesting that the impaired metabolic state contributes to differentiation defects caused by

222 MLL3/4 loss. GO analysis of the 300 significantly rescued genes showed enrichment of genes
223 related to embryo morphogenesis and mesodermal development such as the development of renal
224 and skeletal systems (Fig. 4L). Consistently, HK2/OGDH DOE led to the significant
225 downregulation of pluripotency genes and the significant upregulation of differentiation marker
226 genes (Fig. S5C-D). Taken together, these results suggest that defects in glycolysis and
227 mitochondrial respiration contribute to differentiation failures of naive PSCs lacking MLL3/4.
228

229 **Discussion**

230 Epigenetic regulators, including histone modifiers, play central roles in regulating cell fate
231 transition during PSC differentiation, somatic cell reprogramming, and normal development (*29-*
232 *35*); however, the underlying mechanisms remain incompletely understood, in part because many
233 epigenetic regulators function independently from their catalytic activity (*6, 7, 28, 36-43*). Besides
234 being essential for cellular differentiation and mammalian embryogenesis (*11, 44*), loss-of-
235 function mutations in MLL3 and MLL4 drive congenital disorders such as Kleefstra syndrome 2
236 and Kabuki syndrome, as well as multiple types of cancer (*1, 4, 13, 45*). Recent advances reveal a
237 novel link between MLL3/4 and cellular metabolism; however, whether and how the roles of
238 MLL3/4 in regulating cell fate and metabolic pathways intersect are unclear. Here, we unveil a
239 previously unrecognized function of MLL3/4 in regulating glycolysis and mitochondrial
240 respiration in murine ESCs. Our findings suggest that MLL3/4 govern cell fate transition during
241 the differentiation of naive PSCs through regulating the expression levels of *Hk2* and the function
242 of OGDHc, two rate-limiting nodes in glycolysis and the TCA cycle, respectively. Importantly,
243 restoring defective glycolysis and mitochondrial respiration may be an effective strategy to treat
244 diseases driven by MLL3/MLL4 loss-of-function.

245 We find that MLL3/4 loss causes decreased glycolysis and mitochondrial respiration in
246 ESCs. Metabolic bivalency is a defining feature of naive PSCs such as murine ESCs (*22*). The
247 decrease of glycolysis in MLL3/4-null cells may hinder the cells from exiting naive pluripotency,
248 as formative PSCs and primed PSCs are highly glycolytic (*17*). On the other hand, inhibiting
249 glycolysis promotes differentiation as somatic cells have much elevated levels of oxidative
250 phosphorylation compared with PSCs (*18-20*). Therefore, the dampened mitochondrial respiration
251 caused by MLL3/4 loss may impair the differentiation of PSCs into germ layers and/or specific

252 lineages. Our data provide a mechanistic explanation for the failure of MLL4-null ESCs to exit
253 naive pluripotency and for the severe gastrulation defects observed in MLL3/4-null embryos (*7,*
254 *10, 46*).

255 Our data support that MLL3/4 facilitate glycolysis in naive ESCs through maintaining the
256 expression of *Hk2*, which encodes the rate-limiting enzyme hexokinase 2 in glycolysis. It is
257 possible that MLL3/4 regulate *Hk2* expression through enhancers as we identified multiple
258 putative *cis*-regulatory regions that may be directly regulated by MLL3/4. Understanding whether
259 and how MLL3/4 function through these putative enhancers to control the expression levels of
260 *Hk2* is an interesting topic. Shadow enhancers have been reported in different organisms including
261 *Drosophila*, mouse, and human (*47-49*). Generating individual and compound enhancer mutations
262 will elucidate how the putative enhancers regulate *Hk2*. Combination of MLL3/4 loss-of-function
263 and enhancer mutations will further reveal the functional relationship between MLL3/4 and
264 putative enhancers in regulating *Hk2*. These future studies are essential for understanding the
265 mechanisms by which MLL3/4 regulate glycolysis in naive PSCs.

266 Interestingly, overexpressing HK2 alone only partially restores glycolysis in ESCs lacking
267 MLL3/4, suggesting that MLL3/4 support glycolysis in naive PSCs through additional
268 mechanisms. Determining whether other critical regulators of glycolysis such as
269 phosphofructokinase, pyruvate kinase, and lactate dehydrogenase play a role in dampening
270 glycolysis in the context of MLL3/4 loss-of-function is an important future study. Genome-wide
271 and targeted genetic screens may also identify additional factors that rescue glycolysis in MLL3/4-
272 null ESCs. It is noteworthy that HK2 overexpression leads to a decrease of OCR in MLL3/4 DKO
273 ESCs, suggesting that these cells are more dependent on glycolysis as an energy source in
274 comparison to oxidative phosphorylation under high levels of HK2. Since steady-state acetyl-CoA

275 abundance was reduced in MLL3/4 DKO ESCs (*14*) and our stable isotope tracing assays were not
276 able to detect labeled acetyl-CoA, it is interesting to examine if and how MLL3/4 loss affects the
277 mitochondrial transport of pyruvate in ESCs in the future. Defining the role of MLL3/4 in other
278 pathways leading to the synthesis of acetyl-CoA such as fatty acid metabolism may also facilitate
279 understanding how MLL3/4 regulate the conjunction of glycolysis and the TCA cycle.

280 The reduction in ^{13}C incorporation into succinate, fumarate, and malate in both [$^{13}C_6$]-
281 glucose and [$^{13}C_5$]-glutamine labeling of MLL3/4 DKO ESCs suggests a functionally defective
282 OGDHc caused by MLL3/4 loss. Indeed, the levels of lipoylated DLST were decreased in
283 MLL3/4-null cells, suggesting a reduced activity of the OGDHc. It is likely that the decrease of
284 lipoylation is specific to DLST as MLL3/4 loss has little impact on the levels of lipoylated DLAT.
285 It was previously shown that the α/β hydrolase ABHD11 binds OGDHc and maintains the activity
286 of lipoylated DLST by preventing the formation of lipoyl adducts (*26*). It will be interesting to
287 investigate the functional relationship of MLL3/4, ABHD11, and OGDHc in the future to
288 understand how MLL3/4 regulate the activity of OGDHc. It is also noteworthy that ^{13}C
289 incorporation into α-KG (m+5) is impaired in MLL3/4 DKO ESCs labelled with [$^{13}C_5$]-glutamine,
290 although α-KG (m+2) levels through [$^{13}C_5$]-glucose labeling and steady-state levels of α-KG were
291 largely unchanged by MLL3/4 loss (*14*). Besides glutamate dehydrogenase, glutamate pyruvate
292 transaminase and glutamate oxaloacetate transaminase also can convert glutamate to α-KG.
293 MLL3/4 may also regulate the transport of cytosolic glutamate into mitochondria. Future studies
294 on the role of MLL3/4 in regulating glutamate transport and the conversion of glutamate to α-KG
295 would be important to understand the crosstalk between MLL3/4 and glutaminolysis.

296 α-KG is an essential co-substrate of Fe(II)/α-KG-dependent dioxygenases including
297 Jumonji C (JmjC) domain-containing histone demethylases and the ten-eleven translocation (TET)

298 family of DNA hydroxylases (*50, 51*), playing a role in regulating the levels of methylation on
299 different lysine residues of histones and 5-methyl Cytosine (5mC) on DNA in mammalian cells.
300 Due to their structural similarity to α-KG, 2-hydroxyglutarate, succinate, and fumarate inhibit α-
301 KG-dependent dioxygenases by acting as competitive inhibitors of α-KG (*52, 53*). Our results that
302 MLL3/4 loss in ESCs leads to decreased levels of succinate and fumarate, through steady-state
303 metabolomics (*14*) and stable isotope tracing with [$^{13}C_6$]-glucose and [$^{13}C_5$]-glutamine, suggest a
304 possibility that activities of multiple histone demethylases and TETs are increased in cells with
305 MLL3/4 loss-of-function. Such a possibility provides a mechanistic explanation for the DNA
306 hypomethylation observed in MLL4-depleted B cells in mouse and MLL4 mutant prostate cancers
307 in human (*54*). Understanding the impact of the potential alteration in levels of histone methylation
308 and DNA methylation on the differentiation capability of MLL3/4 mutant PSCs is very interesting
309 and may provide insight into understanding the molecular mechanisms underlying the functional
310 relationship of metabolic state, epigenetic machineries, and cell fate transition.

311 In summary, our study reveals a previously unappreciated crosstalk between epigenetic
312 modifiers exemplified by MLL3/4 and glycolysis and mitochondrial respiration in regulating cell
313 fate. Our findings on MLL3/4 regulating the levels of HK2 and lipoylated DLST could pave the
314 way for designing therapeutic strategies to target human diseases driven by loss-of-function
315 mutations of MLL3/4.
316

317 **Methods**

318 **Antibodies**

319 The following primary antibodies were used in this study: anti-HK2 (Cell Signaling Technology
320 2867), anti-HK1 (Cell Signaling Technology 2024), anti-OGDH (Proteintech 17110-1-AP), anti-
321 SDHA (Abcam 14715), anti-SUCLA2 (Proteintech 12627-1-AP), anti-SUCLG1 (Proteintech
322 14923-1-AP), anti-SUCLG2 (Proteintech NBP1-32521), anti-FLAG (MiliporeSigma F3165),
323 anti-HA (MiliporeSigma H3663), anti-DLST (Cell Signaling Technology 5556), anti-DLD (Santa
324 Cruz 365977), anti-Lipoic acid (Calbiochem 437695), anti-Tubulin (Developmental Studies
325 Hybridoma Bank E7), and anti-HSP90 (Santa Cruz 13119).

326

327 **ESC Culture and EB differentiation**

328 ESCs were cultured in serum-free medium supplemented with 2i/LIF as previously described (*55*).
329 For the generation of HK2 overexpressing and HK2/OGDH DOE MLL3/4 DKO ESCs, cells were
330 transfected with DOX-inducible PiggyBac vectors (*27*) as previously described (*28*) using an
331 Amaxa Nucleofector (Lonza). EB differentiation was performed using the hanging-drop method
332 as previously described (*28*). For DOX-induced overexpression, ESCs were treated with 100 ng/ml
333 doxycycline for 48 hours prior to downstream assays. For differentiation experiments, doxycycline
334 (100 ng/ml) were added 24 hours prior to EB formation and maintained throughout the 6-day
335 differentiation period.

336

337 **Seahorse extracellular flux assays**

338 ESCs were seeded in Seahorse XF microplates (Agilent) and cultured overnight with 2i/LIF serum-
339 free medium. Cells were then incubated in Seahorse XF assay medium (Agilent) at 37°C in a non-

340 CO_2 incubator for 1 hour. For the Glycolysis Stress Test (Agilent 103020-100), glucose (10 mM),
341 oligomycin (2 μM), and 2-DG (50 mM) were sequentially injected. For the Mitochondrial Stress
342 Test (Agilent 103015-100), oligomycin (1.5 μM), FCCP (0.5 μM), and Rot/AA (0.5 μM) were
343 sequentially injected. Cell Titer Glo assay (Promega) was performed in parallel on replica plates
344 to determine the cell number of each well. Individual raw ECAR and OCR values recorded by the
345 Seahorse XF Analyzer were normalized against the average Cell Titer Glo values of control wells
346 to derive normalized ECAR and normalized OCR values. Wave software (Agilent) was used to
347 extract individual ECAR and OCR measurements, which were subsequently used to generate the
348 bar plots.
349
350 **Stable isotope tracing and metabolomics**
351 Stable isotope labeling and metabolite extraction were performed as previously described (*14*).
352 ESCs were incubated with media containing 25 mM [$^{13}C_6$]-glucose or 4 mM [$^{13}C_5$]-glutamine for
353 2 hours before methanol extraction. Metabolomic analyses were performed at the Northwestern
354 Metabolomics Core Facility.
355
356 **Glucose uptake assay**
357 Glucose update was measured using the Glucose Uptake-Glo Assay Kit (Promega J1342)
358 according to the manufacturer's instructions. In brief, 2×10^4 cells were seeded on each well of a
359 96-well flat bottom plate with opaque walls and clear bottoms (Corning 7200587). After 16 hours
360 of culture, cells were incubated in glucose-free medium for 1 hour at 37°C in a CO_2 incubator.
361 Cells were then treated with 1 mM 2-DG for 10 minutes at room temperature, followed by the
362 treatment of stop buffer, neutralization buffer, and detection reagent following the instructions of

363 the manufacturer. After 2.5 hours of dark-conditioned incubation, the luminescence was measured
364 using a GloMax luminometer (Promega). The luminescence data were normalized by cell numbers
365 measured with the Cell Titer Glo assay (Promega) on replica plates in parallel.
366
367 **RNA-seq and analysis**
368 Total RNA was extracted using TRIzol reagent (Thermo Fisher) following the manufacturer's
369 instructions. Each cell line was analyzed in at least two biological replicates. Extracted RNA were
370 treated with DNase I (Sigma) and purified with the RNeasy Plus Mini Kit (Qiagen). Ribosomal
371 RNA was removed from the purified RNA with the NEBNext rRNA Depletion Kit (New England
372 BioLabs). RNA libraries were then prepared with the NEBNext Ultra II Directional RNA Library
373 Prep Kit (New England BioLabs). The pooled libraries were sequenced with 150 bp paired-end
374 reads on the NovaSeq platfrom (Illumina).
375 Raw reads were processed with Trimmomatic v0.39(*56*) to remove adaptors and low-
376 quality reads with the parameter "-q 30". The cleaned reads were aligned to the mm9 genome
377 assembly using STAR v2.5.1 with default parameter (*57*). Reads were normalized to total read
378 counts per million (cpm) and visualized as bigwig-formatted coverage tracks using deepTools
379 v3.5.6 (*58*). Gene expression was quantified using HTseq V2.0.2 (*59*), and differential gene
380 expression analysis was performed with EdgeR v4.0.16 (*60*). Significantly differentially expressed
381 genes were identified with Benjamini-Hochberg-adjusted p value cutoff < 0.01 and a log fold
382 change threshold greater than |1|. hierarchical clustering heatmaps were generated using the ggpubr
383 v0.6.0 (https://rpkgs.datanovia.com/ggpubr/). GSEA plots were generated with clusterProfiler
384 v4.10.1 (*61*). Gene ontology (GO) analysis was performed using Metascape v3.5.20260201 (*62*).
385

Acknowledgements

We thank the Cao lab members for their helpful suggestions and discussions. We thank Dr. Peng Gao and the Northwestern Metabolomics Core Facility for performing the metabolomics study. We thank Emmalee W. Cooke for technical support. We thank Yalu Zhou for bioinformatic analysis support. This study was supported in part by grants R35GM150668, R00HD094906, and P30CA043703 from the National Institutes of Health to K.C.

Author contributions

K.C. conceived the study. S.M.N., I.B., and K.C. designed the research. S.M.N., Y.J., and M.Y. performed experiments. S.M.N., Y.J., M.Y., and K.C. analyzed the data. S.M.N. and K.C. wrote the manuscript. C.A.L. and I.B. critically read the manuscript.

398 **Figure legends**

399 **Figure 1. The loss of MLL3/4 leads to impaired glycolytic activity in ground-state ESCs.**

400 (A) Representative ECAR traces of WT and MLL3/4 DKO ESCs measured by the Seahorse XF
401 glycolysis stress test assay. Data were normalized by the number of cells at the time of the assay
402 and are represented as mean ± S.D. Each data point had six replicates, and the experiment was
403 repeated three times independently. 2-DG: 2-Deoxy-D-glucose.

404 (B-C) Bar plots of ECAR showing the levels of glycolysis (B) and glycolytic capacity (C) in WT
405 and MLL3/4 DKO ESCs. Data are presented as mean ± S.D. p-values were calculated using
406 Student's t-test.

407 (D) Schematic of glycolysis illustrating the fate of ^{13}C carbons upon the incubation with [$^{13}C_6$]-
408 glucose.

409 (E-F) Bar plots showing the levels of F6P/G1P/G6P (m+6, E) and lactate (m+3, F) in WT and
410 MLL3/4 DKO ESCs labeled with [$^{13}C_6$]-glucose. n=3 biological replicates per sample. Data are
411 presented as mean ± S.D. p-values were calculated using Student's t-test.

412 (G) Bar plots showing the levels of glucose uptake in WT and MLL3/4 DKO ESCs. n=6 replicates
413 per sample. Experiments were repeated three times independently and representative results are
414 shown. Data were normalized by the number of cells at the time of the assay and are presented as
415 mean ± S.D. p-values were calculated using Student's t-test. RLU: relative light unit.

416 (H) Western blots showing the levels of HK1 and HK2 in WT and MLL3/4 DKO ESCs. 10 and 20
417 μg of cell lysates were loaded for each sample. Experiments were repeated three times
418 independently and representative results are shown. Protein levels in each lane were quantified by
419 normalizing with Tubulin signals of the corresponding lane.

420

421 **Figure 2. The loss of MLL3/4 leads to impaired mitochondrial respiration in ground-state**
422 **ESCs.**
423 (A) Representative OCR traces of WT and MLL3/4 DKO ESCs measured by the Seahorse XF
424 mitochondrial stress test assay. Data were normalized by the number of cells at the time of the
425 assay and are represented as mean ± S.D. Each data point had six replicates, and the experiment
426 was repeated three times independently. FCCP: Carbonyl Cyanide-4-(trifluoromethoxy)
427 phenylhydrazone. ROT/AA: Rotenone and Antimycin A.
428 (B-C) Bar plots showing the levels of OCR during basal (B) and maximal (C) respiration in WT
429 and MLL3/4 DKO ESCs. Data are presented as mean ± S.D. p-values were calculated using
430 Student's t-test.
431 (D) Schematic of the TCA cycle illustrating the fate of ^{13}C carbons upon the incubation with [$^{13}C_6$]-
432 glucose.
433 (E-I) Bar plots showing levels of citrate/isocitrate (m+2, E), α-KG (m+2, F), succinate (m+2, G),
434 fumarate (m+2, H), and malate (m+2, I) in WT and MLL3/4 DKO ESCs labeled with [$^{13}C_6$]-
435 glucose. n=3 biological replicates per sample. Data are presented as mean ± S.D. p-values were
436 calculated using Student's t-test.
437 (J) Schematic of the TCA cycle illustrating the fate of ^{13}C carbons upon the incubation with [$^{13}C_5$]-
438 glutamine.
439 (K-P) Bar plots showing levels of glutamate (m+5, K), α-KG (m+5, L), succinate (m+4, M),
440 fumarate (m+4, N), malate (m+4, O), and citrate/isocitrate (m+4, P) in WT and MLL3/4 DKO
441 ESCs labeled with [$^{13}C_5$]-glutamine. n=3 biological replicates per sample. Data are presented as
442 mean ± S.D. p-values were calculated using Student's t-test.

443 (Q-T) Western blots showing the levels of OGDH (Q), DLST (R), DLD (S), and lipoylated proteins
444 (T) in WT and MLL3/4 DKO ESCs. 10 and 20 μg of cell lysates were loaded for each sample.
445 Experiments were repeated three times independently and representative results are shown. Protein
446 levels of OGDH (in Q) , DLST (in R), DLD (in S), and lipoylated DLST (in T) were quantified by
447 normalizing with Tubulin or HSP90 signals of the corresponding lane.
448
449 **Figure 3. Combined overexpression of HK2 and OGDH rescues metabolic defects of MLL3/4**
450 **DKO ESCs.**
451 (A) Western blots showing levels of HK2, 3×HA-tagged HK2, OGDH, and 3×FLAG-tagged
452 OGDH in MLL3/4 DKO ESCs and MLL3/4 DKO ESCs overexpressing HK2/OGDH treated with
453 or without DOX. 10 and 20 μg of cell lysates were loaded for each sample. Experiments were
454 repeated three times independently and representative results are shown. Protein levels in each
455 lane of the anti-HK2 and anti-OGDH blots were quantified by normalizing with Tubulin signals
456 of the corresponding lane.
457 (B) Representative ECAR traces of MLL3/4 DKO ESCs treated with DOX (DKO+DOX) and
458 MLL3/4 DKO ESCs overexpressing HK2/OGDH (DOE+DOX) measured by the Seahorse XF
459 glycolysis stress test assay. Data were normalized by the number of cells at the time of the assay
460 and are represented as mean ± S.D. Each data point had six replicates, and the experiment was
461 repeated three times independently.
462 (C-D) Bar plots of ECAR showing the level of glycolysis (C) and glycolytic capacity (D) in
463 MLL3/4 DKO ESCs treated with DOX (DKO+DOX) and MLL3/4 DKO ESCs overexpressing
464 HK2/OGDH (DOE+DOX). Data are presented as mean ± S.D. p-values were calculated using
465 Student's t-test.

466 (E) Representative OCR traces of MLL3/4 DKO ESCs treated with DOX (DKO+DOX) and
467 MLL3/4 DKO ESCs overexpressing HK2/OGDH (DOE+DOX) measured by the Seahorse XF
468 mitochondrial stress test assay. Data were normalized by the number of cells at the time of the
469 assay and are represented as mean ± S.D. Each data point had six replicates, and the experiment
470 was repeated three times independently.
471 (F-G) Bar plots showing the levels of OCR during basal (F) and maximal (G) respiration in
472 MLL3/4 DKO ESCs treated with DOX (DKO+DOX) and MLL3/4 DKO ESCs overexpressing
473 HK2/OGDH (DOE+DOX). Data are presented as mean ± S.D. p-values were calculated using
474 Student's t-test.
475 (H-M) Bar plots showing levels of F6P/G1P/G6P (m+6, H), lactate (m+3, I), α-KG (m+2, J),
476 succinate (m+2, K), fumarate (m+2, L), and malate (m+2, M) in MLL3/4 DKO ESCs treated with
477 DOX (DKO+DOX) and MLL3/4 DKO ESCs overexpressing HK2/OGDH (DOE+DOX) labeled
478 with [$^{13}C_6$]-glucose. n=3 biological replicates per sample. Data are presented as mean ± S.D. p-
479 values were calculated using Student's t-test.
480
481 **Figure 4. Combined overexpression of HK2 and OGDH rescues differentiation defects**
482 **caused by MLL3/4 loss.**
483 (A) Representative images of day 6 WT and MLL3/4 DKO EBs. Scale bar: 250μm.
484 (B) Quantification of EB sizes in (A). n=50 for each genotype. Experiments were repeated three
485 times independently and representative results are shown.
486 (C) Correlation plots of RNA-seq data between day 6 MLL3/4 DKO and WT EBs. Data were
487 derived from two biological replicates. Statistical significance was determined by two-sided Wald
488 test and p-values were corrected for multiple testing using the Benjamini–Hochberg method.

489 Significantly up- and downregulated genes (adjusted $p<0.01$, $|\log FC|>1$) were labeled in red and
490 blue with numbers of genes noted, respectively.
491 (D) Venn diagram identifying 1,192 MLL3/4-dependent differentiation genes.
492 (E) GO analysis of top 300 MLL3/4-dependent differentiation genes.
493 (F) Representative images of day 6 MLL3/4 DKO EBs treated with DOX (DKO+DOX) and
494 MLL3/4 DKO EBs overexpressing HK2/OGDH (DOE+DOX). Scale bar: 250μm.
495 (G) Quantitation of EB sizes in (F). n=50 for each genotype. Experiments were repeated three
496 times independently and representative results are shown.
497 (H) Correlation plots of RNA-seq data between MLL3/4 DKO EBs treated with DOX
498 (DKO+DOX) and MLL3/4 DKO EBs overexpressing HK2/OGDH (DOE+DOX).
499 (I) GSEA analysis of MLL3/4-dependent differentiation genes (1,192 in D) comparing MLL3/4
500 DKO EBs treated with DOX (DKO+DOX) and MLL3/4 DKO EBs overexpressing HK2/OGDH
501 (DOE+DOX). RES: running enrichment score; RLM: ranked list metric; NES: normalized
502 enrichment score; FDR: false discovery rate.
503 (J) Hierarchical clustering analysis of the expression levels of 1,192 MLL3/4-dependent
504 differentiation genes in MLL3/4 DKO EBs treated with DOX (DKO+DOX) and MLL3/4 DKO
505 EBs overexpressing HK2/OGDH (DOE+DOX). FPKM: Fragments per kilobase of transcript per
506 million mapped reads.
507 (K) Venn diagram showing the overlap of MLL3/4-dependent differentiation genes and
508 significantly upregulated genes in MLL3/4 DKO EBs overexpressing HK2/OGDH (red in H).
509 (L) GO analysis of 300 DOE-rescued differentiation genes (overlapping genes in K).
510

511 **Figure S1. The impact of MLL3/4 loss on glycolytic metabolites, glycolytic gene expression,**
512 **and putative enhancers at the *Hk2* locus.**
513 (A-B) Stable isotope tracing of WT and MLL3/4 DKO ESCs labeled with [$^{13}C_6$]-glucose. The
514 levels of isotopologues (m+0 to m+6) of F6P/G6P/G1P (A) and lactate (B) were shown as stacked
515 bar plots.
516 (C) Relative expression levels of genes coding key glycolytic enzymes involved in the production
517 and utilization of G6P, F6P, and lactate. CPM (counts per million reads) from RNA-seq data (*14*)
518 of MLL3/4 DKO ESCs were normalized to those of WT ESCs. p-values were determined by two-
519 sided Wald test and corrected using the Benjamini–Hochberg method.
520 (D) Genome browser view of MLL4 ChIP-seq signals in WT ESCs, and that of H3K27ac and
521 H3K4me3 ChIP-seq signals in WT and MLL3/4 DKO ESCs at the *Hk2* locus. Putative enhancers
522 bound by MLL4 around *Hk2* gene were highlighted.
523
524 **Figure S2. The impact of MLL3/4 loss on TCA cycle metabolites and the expression of TCA**
525 **cycle-related genes.**
526 (A-E) Stable isotope tracing of WT and MLL3/4 DKO ESCs labeled with [$^{13}C_6$]-glucose. The
527 levels of isotopologues (m+0 to m+6) of citrate/isocitrate (A), α-KG (B), succinate (C), fumarate
528 (D), and malate (E) were shown as stacked bar plots.
529 (F-K) Stable isotope tracing of WT and MLL3/4 DKO ESCs labeled with [$^{13}C_5$]-glutamine. The
530 levels of isotopologues (m+0 to m+6) of glutamate (F), α-KG (G), succinate (H), fumarate (I),
531 malate (J), and citrate/isocitrate (K) were shown as stacked bar plots.
532 (L) Relative expression levels of genes coding TCA-cycle enzymes involved in the production and
533 utilization of α-KG, succinate, fumarate, and malate. CPM (counts per million reads) from RNA-

534 seq data (*14*) of MLL3/4 DKO ESCs were normalized to those of WT ESCs. p-values were
535 determined by two-sided Wald test and corrected using the Benjamini–Hochberg method.
536 (M-N) Western blots showing levels of Succinyl-CoA Synthetase subunits (M), SDHA (N, top
537 blot), and FH (N, middle blot). 10 and 20 μg of cell lysates were loaded for each sample.
538 Experiments were repeated three times independently and representative results are shown. Protein
539 levels in each lane were quantified by normalizing with HSP90 signals of the corresponding lane.
540

541 **Figure S3. HK2 overexpression leads to an increase in glycolysis but a decrease in**
542 **mitochondrial respiration in MLL3/4 DKO ESCs.**
543 (A) Western blots showing the induction of 3×HA-tagged HK2 in HK2-overexpressing MLL3/4
544 DKO ESCs by DOX. 10 and 20 μg of cell lysates were loaded for each sample. Experiments were
545 repeated three times independently and representative results are shown. Protein levels of HK2 in
546 each lane were quantified by normalizing with Tubulin signals of the corresponding lane.
547 (B) Representative ECAR traces of MLL3/4 DKO ESCs treated with DOX (DKO+DOX) and
548 MLL3/4 DKO ESCs overexpressing HK2 (3×HA-HK2+DOX) measured by the Seahorse XF
549 glycolysis stress test assay. Data were normalized by the number of cells at the time of the assay
550 and are represented as mean ± S.D. Each data point had six replicates, and the experiment was
551 repeated three times independently.
552 (C-D) Bar plots of ECAR showing the levels of glycolysis (C) and glycolytic capacity (D) in
553 MLL3/4 DKO ESCs treated with DOX (DKO+DOX) and MLL3/4 DKO ESCs overexpressing
554 HK2 (3×HA-HK2+DOX). Data are presented as mean ± S.D. p-values were calculated using
555 Student's t-test.

556 (E) Representative OCR traces of MLL3/4 DKO ESCs treated with DOX (DKO+DOX) and
557 MLL3/4 DKO ESCs overexpressing HK2 (3×HA-HK2+DOX) measured by the Seahorse XF
558 mitochondrial stress test assay. Data were normalized by the number of cells at the time of the
559 assay and are represented as mean ± S.D. Each data point had six replicates, and the experiment
560 was repeated three times independently.
561 (F-G) Bar plots showing the OCR levels in MLL3/4 DKO ESCs treated with DOX (DKO+DOX)
562 and MLL3/4 DKO ESCs overexpressing HK2 (3×HA-HK2+DOX) during basal (F) and maximal
563 (G) respiration. Data are presented as mean ± S.D. p-values were calculated using Student's t-test.
564
565 **Figure S4. Stable isotope tracing of MLL3/4 DKO ESCs treated with DOX (DKO+DOX) and**
566 **MLL3/4 DKO ESCs overexpressing HK2/OGDH (DOE+DOX) labeled with [$^{13}C_6$]-glucose.**
567 The levels of isotopologues of F6P/G1P/G6P (A, m+0 to m+6), lactate (B m+0 to m+3),
568 citrate/isocitrate (m+2 in C and m+0 to m+6 in D), α-KG (E, m+0 to m+5), succinate (F, m+0 to
569 m+4), fumarate (G, m+0 to m+4), and malate (H, m+0 to m+4) were shown.
570
571 **Figure S5. The impact of MLL3/4 loss and HK2/OGDH overexpression on the expression**
572 **levels of marker genes of pluripotency and differentiation in EBs.**
573 (A-B) Relative expression levels of pluripotency genes (A) and differentiation markers (B) in
574 MLL3/4 DKO EBs compared with WT EBs. Log2 fold change of RNA-seq signals (CPM) were
575 shown. Data are presented as mean values ± SD. n = 2 biologically independent experiments. All
576 p-values were smaller than 0.01 compared with WT EBs.
577 (C-D) Relative expression levels of pluripotency genes (C) and differentiation markers (D) in
578 MLL3/4 DKO EBs overexpressing HK2/OGDH (DOE+DOX) compared with MLL3/4 DKO EBs

579 treated with DOX (DKO+DOX). Log2 fold change of RNA-seq signals (CPM) were shown. Data
580 are presented as mean values ± SD. n = 2 biologically independent experiments. All p-values were
581 smaller than 0.01 compared with DKO+DOX EBs.
582

583 **References**

584 1. S. B. Ng, A. W. Bigham, K. J. Buckingham, M. C. Hannibal, M. J. McMillin, H. I.
585 Gildersleeve, A. E. Beck, H. K. Tabor, G. M. Cooper, H. C. Mefford, C. Lee, E. H. Turner,
586 J. D. Smith, M. J. Rieder, K. Yoshiura, N. Matsumoto, T. Ohta, N. Niikawa, D. A.
587 Nickerson, M. J. Bamshad, J. Shendure, Exome sequencing identifies MLL2 mutations
588 as a cause of Kabuki syndrome. *Nat Genet* **42**, 790-793 (2010).
589 2. I. D. Krantz, J. McCallum, C. DeScipio, M. Kaur, L. A. Gillis, D. Yaeger, L. Jukofsky, N.
590 Wasserman, A. Bottani, C. A. Morris, M. J. Nowaczyk, H. Toriello, M. J. Bamshad, J. C.
591 Carey, E. Rappaport, S. Kawauchi, A. D. Lander, A. L. Calof, H. H. Li, M. Devoto, L. G.
592 Jackson, Cornelia de Lange syndrome is caused by mutations in NIPBL, the human
593 homolog of Drosophila melanogaster Nipped-B. *Nat Genet* **36**, 631-635 (2004).
594 3. E. K. Schorry, M. Keddache, N. Lanphear, J. H. Rubinstein, S. Srodulski, D. Fletcher, R.
595 I. Blough-Pfau, G. A. Grabowski, Genotype-phenotype correlations in Rubinstein-
596 Taybi syndrome. *Am J Med Genet A* **146A**, 2512-2519 (2008).
597 4. T. S. Koemans, T. Kleefstra, M. C. Chubak, M. H. Stone, M. R. F. Reijnders, S. de Munnik,
598 M. H. Willemsen, M. Fenckova, C. Stumpel, L. A. Bok, M. Sifuentes Saenz, K. A. Byerly,
599 L. B. Baughn, A. P. A. Stegmann, R. Pfundt, H. Zhou, H. van Bokhoven, A. Schenck, J.
600 M. Kramer, Functional convergence of histone methyltransferases EHMT1 and
601 KMT2C involved in intellectual disability and autism spectrum disorder. *PLoS Genet*
602 **13**, e1006864 (2017).
603 5. D. Hu, X. Gao, M. A. Morgan, H. M. Herz, E. R. Smith, A. Shilatifard, The MLL3/MLL4
604 branches of the COMPASS family function as major histone H3K4 monomethylases
605 at enhancers. *Mol Cell Biol* **33**, 4745-4754 (2013).
606 6. R. Rickels, H. M. Herz, C. C. Sze, K. Cao, M. A. Morgan, C. K. Collings, M. Gause, Y. H.
607 Takahashi, L. Wang, E. J. Rendleman, S. A. Marshall, A. Krueger, E. T. Bartom, A. Piunti,
608 E. R. Smith, N. A. Abshiru, N. L. Kelleher, D. Dorsett, A. Shilatifard, Histone H3K4
609 monomethylation catalyzed by Trr and mammalian COMPASS-like proteins at
610 enhancers is dispensable for development and viability. *Nat Genet* **49**, 1647-1653
611 (2017).
612 7. K. Cao, C. K. Collings, M. A. Morgan, S. A. Marshall, E. J. Rendleman, P. A. Ozark, E. R.
613 Smith, A. Shilatifard, An Mll4/COMPASS-Lsd1 epigenetic axis governs enhancer
614 function and pluripotency transition in embryonic stem cells. *Sci Adv* **4**, eaap8747
615 (2018).
616 8. A. Shilatifard, The COMPASS family of histone H3K4 methylases: mechanisms of
617 regulation in development and disease pathogenesis. *Annu Rev Biochem* **81**, 65-95
618 (2012).
619 9. N. D. Heintzman, R. K. Stuart, G. Hon, Y. Fu, C. W. Ching, R. D. Hawkins, L. O. Barrera,
620 S. Van Calcar, C. Qu, K. A. Ching, W. Wang, Z. Weng, R. D. Green, G. E. Crawford, B.
621 Ren, Distinct and predictive chromatin signatures of transcriptional promoters and
622 enhancers in the human genome. *Nat Genet* **39**, 311-318 (2007).
623 10. J. E. Lee, C. Wang, S. Xu, Y. W. Cho, L. Wang, X. Feng, A. Baldridge, V. Sartorelli, L.
624 Zhuang, W. Peng, K. Ge, H3K4 mono- and di-methyltransferase MLL4 is required for
625 enhancer activation during cell differentiation. *Elife* **2**, e01503 (2013).

11. D. Ashokkumar, Q. Zhang, C. Much, A. S. Bledau, R. Naumann, D. Alexopoulou, A. Dahl, N. Goveas, J. Fu, K. Anastassiadis, A. F. Stewart, A. Kranz, MLL4 is required after implantation, whereas MLL3 becomes essential during late gestation. *Development* **147**, (2020).
12. V. Faundes, W. G. Newman, L. Bernardini, N. Canham, J. Clayton-Smith, B. Dallapiccola, S. J. Davies, M. K. Demos, A. Goldman, H. Gill, R. Horton, B. Kerr, D. Kumar, A. Lehman, S. McKee, J. Morton, M. J. Parker, J. Rankin, L. Robertson, I. K. Temple, S. Clinical Assessment of the Utility of, S. Evaluation as a Service, S. Deciphering Developmental Disorders, S. Banka, Histone Lysine Methylases and Demethylases in the Landscape of Human Developmental Disorders. *Am J Hum Genet* **102**, 175-187 (2018).
13. D. Rots, S. Choufani, V. Faundes, A. J. M. Dingemans, S. Joss, N. Foulds, E. A. Jones, S. Stewart, P. Vasudevan, T. Dabir, S. M. Park, R. Jewell, N. Brown, L. Pais, S. Jacquemont, K. Jizi, C. Ravenswaaij-Arts, H. Y. Kroes, C. Stumpel, C. W. Ockeloen, I. J. Diets, M. Nizon, M. Vincent, B. Cogne, T. Besnard, M. Kambouris, E. Anderson, E. H. Zackai, C. McDougall, S. Donoghue, A. O'Donnell-Luria, Z. Valivullah, M. O'Leary, S. Srivastava, H. Byers, N. Leslie, S. Mazzola, G. E. Tiller, M. Vera, J. J. Shen, R. Boles, V. Jain, E. Brischoux-Boucher, E. Kinning, B. N. Simpson, J. C. Giltay, J. Harris, B. Keren, A. Guimier, P. Marijon, B. B. A. Vries, C. S. Motter, B. A. Mendelsohn, S. Coffino, E. H. Gerkes, A. Afenjar, P. Visconti, E. Bacchelli, E. Maestrini, A. Delahaye-Duriez, C. Gooch, Y. Hendriks, H. Adams, C. Thauvin-Robinet, S. Josephi-Taylor, M. Bertoli, M. J. Parker, J. W. Rutten, O. Caluseriu, H. J. Vernon, J. Kaziyev, J. Zhu, J. Kremen, Z. Frazier, H. Osika, D. Breault, S. Nair, S. M. E. Lewis, F. Ceroni, M. Viggiano, A. Posar, H. Brittain, T. Giovanna, G. Giulia, L. Quteineh, R. Ha-Vinh Leuchter, E. Zonneveld-Huijssoon, C. Mellado, I. Marey, A. Coudert, M. I. Aracena Alvarez, M. G. P. Kennis, A. Bouman, M. Roifman, M. I. Amoros Rodriguez, J. D. Ortigoza-Escobar, V. Vernimmen, M. Sinnema, R. Pfundt, H. G. Brunner, L. Vissers, T. Kleefstra, R. Weksberg, S. Banka, Pathogenic variants in KMT2C result in a neurodevelopmental disorder distinct from Kleefstra and Kabuki syndromes. *Am J Hum Genet* **111**, 1626-1642 (2024).
14. Z. Zhao, K. Cao, J. Watanabe, C. N. Philips, J. M. Zeidner, Y. Ishi, Q. Wang, S. R. Gold, K. Junkins, E. T. Bartom, F. Yue, N. S. Chandel, R. Hashizume, I. Ben-Sahra, A. Shilatifard, Therapeutic targeting of metabolic vulnerabilities in cancers with MLL3/4-COMPASS epigenetic regulator mutations. *J Clin Invest* **133**, (2023).
15. H. Alam, M. Tang, M. Maitituoheti, S. S. Dhar, M. Kumar, C. Y. Han, C. R. Ambati, S. B. Amin, B. Gu, T. Y. Chen, Y. H. Lin, J. Chen, F. L. Muller, N. Putluri, E. R. Flores, F. J. DeMayo, L. Baseler, K. Rai, M. G. Lee, KMT2D Deficiency Impairs Super-Enhancers to Confer a Glycolytic Vulnerability in Lung Cancer. *Cancer Cell* **37**, 599-617 e597 (2020).
16. M. Maitituoheti, E. Z. Keung, M. Tang, L. Yan, H. Alam, G. Han, A. K. Singh, A. T. Raman, C. Terranova, S. Sarkar, E. Orouji, S. B. Amin, S. Sharma, M. Williams, N. S. Samant, M. Dhamdhere, N. Zheng, T. Shah, A. Shah, J. B. Axelrad, N. E. Anvar, Y. H. Lin, S. Jiang, E. Q. Chang, D. R. Ingram, W. L. Wang, A. Lazar, M. G. Lee, F. Muller, L. Wang, H. Ying, K. Rai, Enhancer Reprogramming Confers Dependence on Glycolysis and IGF Signaling in KMT2D Mutant Melanoma. *Cell Rep* **33**, 108293 (2020).

669 17. W. Zhou, M. Choi, D. Margineantu, L. Margaretha, J. Hesson, C. Cavanaugh, C. A. Blau,
670 M. S. Horwitz, D. Hockenbery, C. Ware, H. Ruohola-Baker, HIF1alpha induced switch
671 from bivalent to exclusively glycolytic metabolism during ESC-to-EpiSC/hESC
672 transition. *EMBO J* **31**, 2103-2116 (2012).
673 18. C. D. Folmes, T. J. Nelson, A. Martinez-Fernandez, D. K. Arrell, J. Z. Lindor, P. P. Dzeja,
674 Y. Ikeda, C. Perez-Terzic, A. Terzic, Somatic oxidative bioenergetics transitions into
675 pluripotency-dependent glycolysis to facilitate nuclear reprogramming. *Cell Metab*
676 **14**, 264-271 (2011).
677 19. A. D. Panopoulos, O. Yanes, S. Ruiz, Y. S. Kida, D. Diep, R. Tautenhahn, A. Herrerias,
678 E. M. Batchelder, N. Plongthongkum, M. Lutz, W. T. Berggren, K. Zhang, R. M. Evans,
679 G. Siuzdak, J. C. Izpisua Belmonte, The metabolome of induced pluripotent stem cells
680 reveals metabolic changes occurring in somatic cell reprogramming. *Cell Res* **22**,
681 168-177 (2012).
682 20. A. Moussaieff, M. Rouleau, D. Kitsberg, M. Cohen, G. Levy, D. Barasch, A. Nemirovski,
683 S. Shen-Orr, I. Laevsky, M. Amit, D. Bomze, B. Elena-Herrmann, T. Scherf, M. Nissim-
684 Rafinia, S. Kempa, J. Itskovitz-Eldor, E. Meshorer, D. Aberdam, Y. Nahmias, Glycolysis-
685 mediated changes in acetyl-CoA and histone acetylation control the early
686 differentiation of embryonic stem cells. *Cell Metab* **21**, 392-402 (2015).
687 21. A. De Los Angeles, F. Ferrari, R. Xi, Y. Fujiwara, N. Benvenisty, H. Deng, K.
688 Hochedlinger, R. Jaenisch, S. Lee, H. G. Leitch, M. W. Lensch, E. Lujan, D. Pei, J.
689 Rossant, M. Wernig, P. J. Park, G. Q. Daley, Hallmarks of pluripotency. *Nature* **525**,
690 469-478 (2015).
691 22. P. Du, J. Wu, Hallmarks of totipotent and pluripotent stem cell states. *Cell Stem Cell*
692 **31**, 312-333 (2024).
693 23. E. A. Rowland, T. M. Greco, C. K. Snowden, A. L. McCabe, T. J. Silhavy, I. M. Cristea,
694 Sirtuin Lipoamidase Activity Is Conserved in Bacteria as a Regulator of Metabolic
695 Enzyme Complexes. *mBio* **8**, (2017).
696 24. E. A. Rowland, C. K. Snowden, I. M. Cristea, Protein lipoylation: an evolutionarily
697 conserved metabolic regulator of health and disease. *Curr Opin Chem Biol* **42**, 76-85
698 (2018).
699 25. J. E. Cronan, Assembly of Lipoic Acid on Its Cognate Enzymes: an Extraordinary and
700 Essential Biosynthetic Pathway. *Microbiol Mol Biol Rev* **80**, 429-450 (2016).
701 26. P. S. J. Bailey, B. M. Ortmann, A. W. Martinelli, J. W. Houghton, A. S. H. Costa, S. P. Burr,
702 R. Antrobus, C. Frezza, J. A. Nathan, ABHD11 maintains 2-oxoglutarate metabolism
703 by preserving functional lipoylation of the 2-oxoglutarate dehydrogenase complex.
704 *Nat Commun* **11**, 4046 (2020).
705 27. C. Buecker, R. Srinivasan, Z. Wu, E. Calo, D. Acampora, T. Faial, A. Simeone, M. Tan,
706 T. Swigut, J. Wysocka, Reorganization of enhancer patterns in transition from naive to
707 primed pluripotency. *Cell Stem Cell* **14**, 838-853 (2014).
708 28. C. Zeng, J. Chen, E. W. Cooke, A. Subuddhi, E. T. Roodman, F. X. Chen, K. Cao,
709 Demethylase-independent roles of LSD1 in regulating enhancers and cell fate
710 transition. *Nat Commun* **14**, 4944 (2023).
711 29. J. A. Lessard, G. R. Crabtree, Chromatin regulatory mechanisms in pluripotency. *Annu*
712 *Rev Cell Dev Biol* **26**, 503-532 (2010).

30. S. Feng, S. E. Jacobsen, W. Reik, Epigenetic reprogramming in plant and animal development. *Science* **330**, 622-627 (2010).
31. B. Papp, K. Plath, Epigenetics of reprogramming to induced pluripotency. *Cell* **152**, 1324-1343 (2013).
32. W. W. Tee, D. Reinberg, Chromatin features and the epigenetic regulation of pluripotency states in ESCs. *Development* **141**, 2376-2390 (2014).
33. S. Schlesinger, E. Meshorer, Open Chromatin, Epigenetic Plasticity, and Nuclear Organization in Pluripotency. *Dev Cell* **48**, 135-150 (2019).
34. A. Burton, M. E. Torres-Padilla, Epigenome dynamics in early mammalian embryogenesis. *Nat Rev Genet* **26**, 587-603 (2025).
35. X. Wan, S. Zhang, J. Li, D. Kong, M. Chen, Epigenetic remodeling during early embryonic development. *Front Cell Dev Biol* **14**, 1750381 (2026).
36. R. Eskeland, M. Leeb, G. R. Grimes, C. Kress, S. Boyle, D. Sproul, N. Gilbert, Y. Fan, A. I. Skoultchi, A. Wutz, W. A. Bickmore, Ring1B compacts chromatin structure and represses gene expression independent of histone ubiquitination. *Mol Cell* **38**, 452-464 (2010).
37. R. S. Illingworth, M. Moffat, A. R. Mann, D. Read, C. J. Hunter, M. M. Pradeepa, I. R. Adams, W. A. Bickmore, The E3 ubiquitin ligase activity of RING1B is not essential for early mouse development. *Genes Dev* **29**, 1897-1902 (2015).
38. C. C. Sze, K. Cao, C. K. Collings, S. A. Marshall, E. J. Rendleman, P. A. Ozark, F. X. Chen, M. A. Morgan, L. Wang, A. Shilatifard, Histone H3K4 methylation-dependent and -independent functions of Set1A/COMPASS in embryonic stem cell self-renewal and differentiation. *Genes Dev* **31**, 1732-1737 (2017).
39. L. Wang, C. K. Collings, Z. Zhao, K. A. Cozzolino, Q. Ma, K. Liang, S. A. Marshall, C. C. Sze, R. Hashizume, J. N. Savas, A. Shilatifard, A cytoplasmic COMPASS is necessary for cell survival and triple-negative breast cancer pathogenesis by regulating metabolism. *Genes Dev* **31**, 2056-2066 (2017).
40. K. M. Dorighi, T. Swigut, T. Henriques, N. V. Bhanu, B. S. Scruggs, N. Nady, C. D. Still, 2nd, B. A. Garcia, K. Adelman, J. Wysocka, Mll3 and Mll4 Facilitate Enhancer RNA Synthesis and Transcription from Promoters Independently of H3K4 Monomethylation. *Mol Cell* **66**, 568-576 e564 (2017).
41. K. Cao, M. Ugarenko, P. A. Ozark, J. Wang, S. A. Marshall, E. J. Rendleman, K. Liang, L. Wang, L. Zou, E. R. Smith, F. Yue, A. Shilatifard, DOT1L-controlled cell-fate determination and transcription elongation are independent of H3K79 methylation. *Proc Natl Acad Sci U S A* **117**, 27365-27373 (2020).
42. M. A. J. Morgan, A. Shilatifard, Epigenetic moonlighting: Catalytic-independent functions of histone modifiers in regulating transcription. *Sci Adv* **9**, eadg6593 (2023).
43. A. Khan, C. Zhang, P. G. Nguyen, J. M. Metts, L. C. Collins, K. Jain, C. A. Mills, L. Vlach, K. Li, A. L. Brademeyer, B. M. Bowman, M. B. Major, J. Aube, L. E. Herring, W. K. Rathmell, F. M. Mason, I. J. Davis, Q. Zhang, B. D. Strahl, A SETD2-CDK1-lamin axis maintains nuclear morphology and genome stability. *Nat Cell Biol* **27**, 1327-1341 (2025).

44. C. Wang, J. E. Lee, B. Lai, T. S. Macfarlan, S. Xu, L. Zhuang, C. Liu, W. Peng, K. Ge, Enhancer priming by H3K4 methyltransferase MLL4 controls cell fate transition. *Proc Natl Acad Sci U S A* **113**, 11871-11876 (2016).
45. C. C. Sze, A. Shilatifard, MLL3/MLL4/COMPASS Family on Epigenetic Regulation of Enhancer Function and Cancer. *Cold Spring Harb Perspect Med* **6**, (2016).
46. G. Xie, J. E. Lee, A. D. Senft, Y. K. Park, Y. Jang, S. Chakraborty, J. J. Thompson, K. McKernan, C. Liu, T. S. Macfarlan, P. P. Rocha, W. Peng, K. Ge, MLL3/MLL4 methyltransferase activities control early embryonic development and embryonic stem cell differentiation in a lineage-selective manner. *Nat Genet* **55**, 693-705 (2023).
47. J. W. Hong, D. A. Hendrix, M. S. Levine, Shadow enhancers as a source of evolutionary novelty. *Science* **321**, 1314 (2008).
48. K. Cao, C. K. Collings, S. A. Marshall, M. A. Morgan, E. J. Rendleman, L. Wang, C. C. Sze, T. Sun, E. T. Bartom, A. Shilatifard, SET1A/COMPASS and shadow enhancers in the regulation of homeotic gene expression. *Genes Dev* **31**, 787-801 (2017).
49. E. Z. Kvon, R. Waymack, M. Gad, Z. Wunderlich, Enhancer redundancy in development and disease. *Nat Rev Genet* **22**, 324-336 (2021).
50. Y. Tsukada, J. Fang, H. Erdjument-Bromage, M. E. Warren, C. H. Borchers, P. Tempst, Y. Zhang, Histone demethylation by a family of JmjC domain-containing proteins. *Nature* **439**, 811-816 (2006).
51. M. Tahiliani, K. P. Koh, Y. Shen, W. A. Pastor, H. Bandukwala, Y. Brudno, S. Agarwal, L. M. Iyer, D. R. Liu, L. Aravind, A. Rao, Conversion of 5-methylcytosine to 5-hydroxymethylcytosine in mammalian DNA by MLL partner TET1. *Science* **324**, 930-935 (2009).
52. W. Xu, H. Yang, Y. Liu, Y. Yang, P. Wang, S. H. Kim, S. Ito, C. Yang, P. Wang, M. T. Xiao, L. X. Liu, W. Q. Jiang, J. Liu, J. Y. Zhang, B. Wang, S. Frye, Y. Zhang, Y. H. Xu, Q. Y. Lei, K. L. Guan, S. M. Zhao, Y. Xiong, Oncometabolite 2-hydroxyglutarate is a competitive inhibitor of alpha-ketoglutarate-dependent dioxygenases. *Cancer Cell* **19**, 17-30 (2011).
53. M. Xiao, H. Yang, W. Xu, S. Ma, H. Lin, H. Zhu, L. Liu, Y. Liu, C. Yang, Y. Xu, S. Zhao, D. Ye, Y. Xiong, K. L. Guan, Inhibition of alpha-KG-dependent histone and DNA demethylases by fumarate and succinate that are accumulated in mutations of FH and SDH tumor suppressors. *Genes Dev* **26**, 1326-1338 (2012).
54. K. Skvortsova, E. Masle-Farquhar, P. L. Luu, J. Z. Song, W. Qu, E. Zotenko, C. M. Gould, Q. Du, T. J. Peters, Y. Colino-Sanguino, R. Pidsley, S. S. Nair, A. Khoury, G. C. Smith, L. A. Miosge, J. H. Reed, J. G. Kench, M. A. Rubin, L. Horvath, O. Bogdanovic, S. M. Lim, J. M. Polo, C. C. Goodnow, C. Stirzaker, S. J. Clark, DNA Hypermethylation Encroachment at CpG Island Borders in Cancer Is Predisposed by H3K4 Monomethylation Patterns. *Cancer Cell* **35**, 297-314 e298 (2019).
55. E. W. Cooke, C. Zeng, S. M. Nur, Y. Jia, A. Huang, J. Chen, P. Gao, F. X. Chen, F. Jin, K. Cao, H3K79 methylation and H3K36 trimethylation synergistically regulate gene expression in pluripotent stem cells. *Sci Adv* **11**, eadt8765 (2025).
56. A. M. Bolger, M. Lohse, B. Usadel, Trimmomatic: a flexible trimmer for Illumina sequence data. *Bioinformatics* **30**, 2114-2120 (2014).

57. A. Dobin, C. A. Davis, F. Schlesinger, J. Drenkow, C. Zaleski, S. Jha, P. Batut, M. Chaisson, T. R. Gingeras, STAR: ultrafast universal RNA-seq aligner. *Bioinformatics* **29**, 15-21 (2013).
58. F. Ramirez, D. P. Ryan, B. Gruning, V. Bhardwaj, F. Kilpert, A. S. Richter, S. Heyne, F. Dundar, T. Manke, deepTools2: a next generation web server for deep-sequencing data analysis. *Nucleic Acids Res* **44**, W160-165 (2016).
59. S. Anders, P. T. Pyl, W. Huber, HTSeq--a Python framework to work with high-throughput sequencing data. *Bioinformatics* **31**, 166-169 (2015).
60. M. D. Robinson, D. J. McCarthy, G. K. Smyth, edgeR: a Bioconductor package for differential expression analysis of digital gene expression data. *Bioinformatics* **26**, 139-140 (2010).
61. T. Wu, E. Hu, S. Xu, M. Chen, P. Guo, Z. Dai, T. Feng, L. Zhou, W. Tang, L. Zhan, X. Fu, S. Liu, X. Bo, G. Yu, clusterProfiler 4.0: A universal enrichment tool for interpreting omics data. *Innovation (Camb)* **2**, 100141 (2021).
62. Y. Zhou, B. Zhou, L. Pache, M. Chang, A. H. Khodabakhshi, O. Tanaseichuk, C. Benner, S. K. Chanda, Metascape provides a biologist-oriented resource for the analysis of systems-level datasets. *Nat Commun* **10**, 1523 (2019).

Figure 1

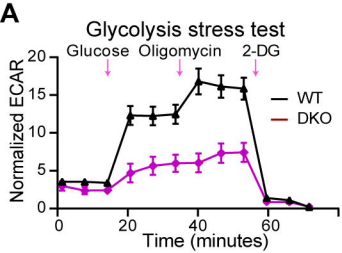
A
Glycolysis stress test
Glucose
Oligomycin
2-DG
Normalized ECAR
Time (minutes)
WT
DKO

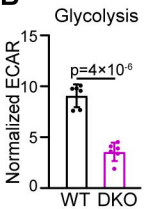
B
Glycolysis
Normalized ECAR
p=4×10-6
WT
DKO

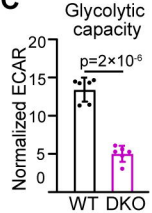
C
Glycolytic capacity
Normalized ECAR
p=2×10-6
WT
DKO

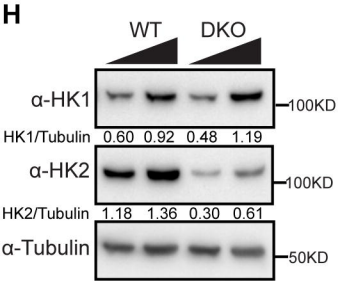
H
WT
DKO
α-HK1
100KD
HK1/Tubulin
0.60
0.92
0.48
1.19
α-HK2
100KD
HK2/Tubulin
1.18
1.36
0.30
0.61
α-Tubulin
50KD

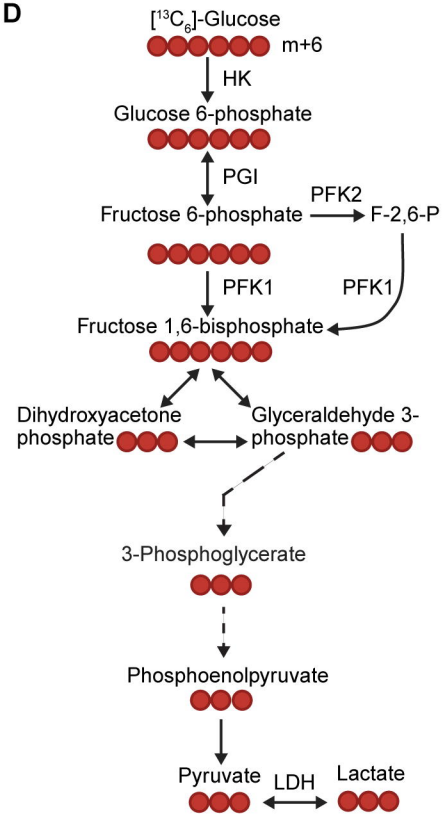
D
[13C6]-Glucose
m+6
HK
Glucose 6-phosphate
PGI
Fructose 6-phosphate
PFK2
F-2,6-P
PFK1
PFK1
Fructose 1,6-bisphosphate
Dihydroxyacetone phosphate
Glyceraldehyde 3-phosphate
3-Phosphoglycerate
Phosphoenolpyruvate
Pyruvate
LDH
Lactate

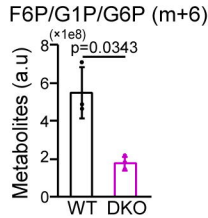
E
F6P/G1P/G6P (m+6)
(×1e8)
p=0.0343
Metabolites (a.u)
WT
DKO

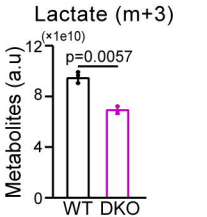
F
Lactate (m+3)
(×1e10)
p=0.0057
Metabolites (a.u)
WT
DKO

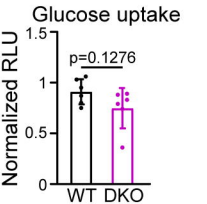
G
Glucose uptake
p=0.1276
Normalized RLU
WT
DKO

Figure 2

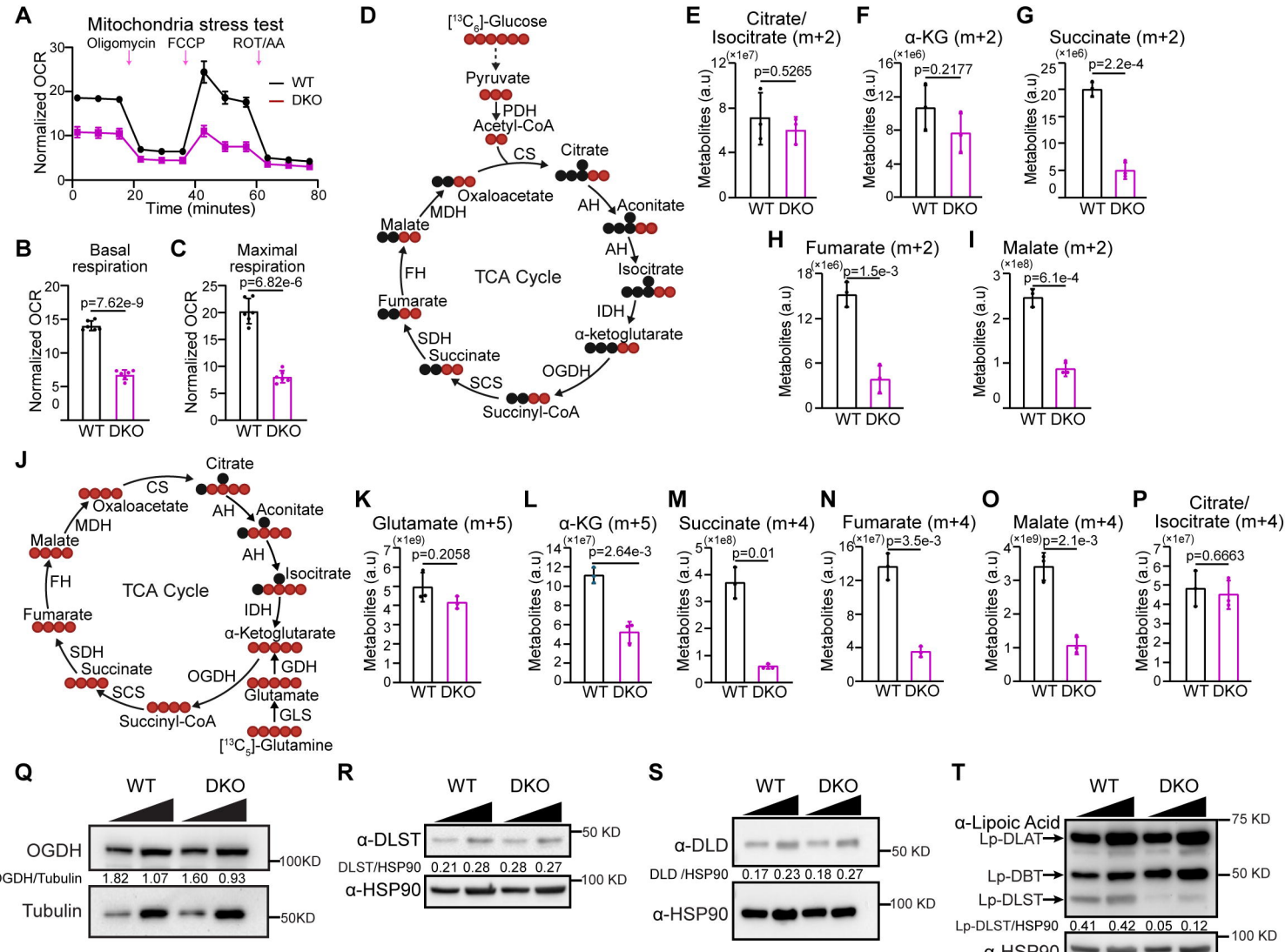
A
Mitochondria stress test
Oligomycin
FCCP
ROT/AA
Normalized OCR
Time (minutes)
WT
DKO
B
Basal respiration
p=7.62e-9
C
Maximal respiration
p=6.82e-6
D
[13C6]-Glucose
Pyruvate
PDH
Acetyl-CoA
CS
Citrate
Oxaloacetate
MDH
Malate
AH
Aconitate
AH
Isocitrate
IDH
α-ketoglutarate
OGDH
Succinyl-CoA
SCS
Succinate
SDH
Fumarate
FH
TCA Cycle
E
Citrate/ Isocitrate (m+2)
p=0.5265
F
α-KG (m+2)
p=0.2177
G
Succinate (m+2)
p=2.2e-4
H
Fumarate (m+2)
p=1.5e-3
I
Malate (m+2)
p=6.1e-4
Metabolites (a.u)
J
[13C5]-Glutamine
GLS
Glutamate
GDH
K
Glutamate (m+5)
p=0.2058
L
α-KG (m+5)
p=2.64e-3
M
Succinate (m+4)
p=0.01
N
Fumarate (m+4)
p=3.5e-3
O
Malate (m+4)
p=2.1e-3
P
Citrate/ Isocitrate (m+4)
p=0.6663
Q
OGDH
OGDH/Tubulin
1.82 1.07 1.60 0.93
Tubulin
100KD
50KD
R
α-DLST
DLST/HSP90
0.21 0.28 0.28 0.27
α-HSP90
50 KD
100 KD
S
α-DLD
DLD /HSP90
0.17 0.23 0.18 0.27
T
α-Lipoic Acid
Lp-DLAT
Lp-DBT
Lp-DLST
Lp-DLST/HSP90
0.41 0.42 0.05 0.12
75 KD

Figure 3

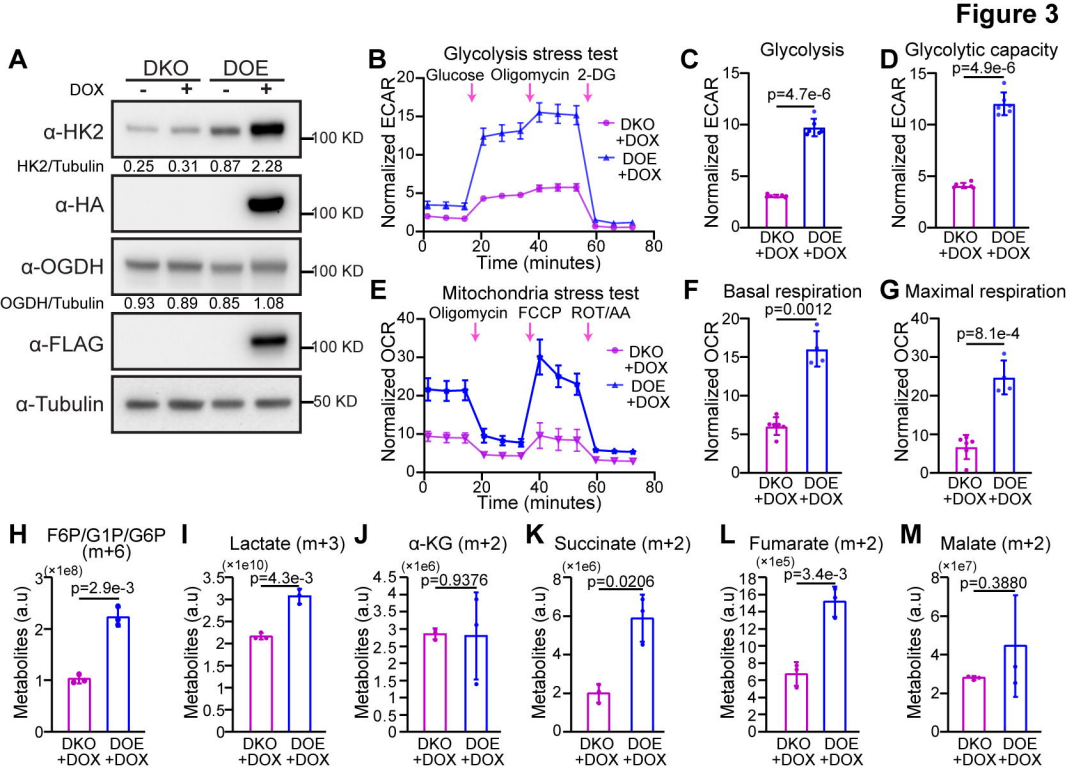
A
DKO
DOE
DOX
- + - +
α-HK2
100 KD
HK2/Tubulin
0.25 0.31 0.87 2.28
α-HA
100 KD
α-OGDH
100 KD
OGDH/Tubulin
0.93 0.89 0.85 1.08
α-FLAG
100 KD
α-Tubulin
50 KD
B
Glycolysis stress test
Glucose Oligomycin 2-DG
Normalized ECAR
Time (minutes)
DKO +DOX
DOE +DOX
C
Glycolysis
p=4.7e-6
Normalized ECAR
D
Glycolytic capacity
p=4.9e-6
Normalized ECAR
E
Mitochondria stress test
Oligomycin FCCP ROT/AA
Normalized OCR
Time (minutes)
F
Basal respiration
p=0.0012
Normalized OCR
G
Maximal respiration
p=8.1e-4
Normalized OCR
H
F6P/G1P/G6P (m+6)
(×1e8)
p=2.9e-3
Metabolites (a.u)
I
Lactate (m+3)
(×1e10)
p=4.3e-3
Metabolites (a.u)
J
α-KG (m+2)
(×1e6)
p=0.9376
Metabolites (a.u)
K
Succinate (m+2)
(×1e6)
p=0.0206
Metabolites (a.u)
L
Fumarate (m+2)
(×1e5)
p=3.4e-3
Metabolites (a.u)
M
Malate (m+2)
(×1e7)
p=0.3880
Metabolites (a.u)

Figure 4

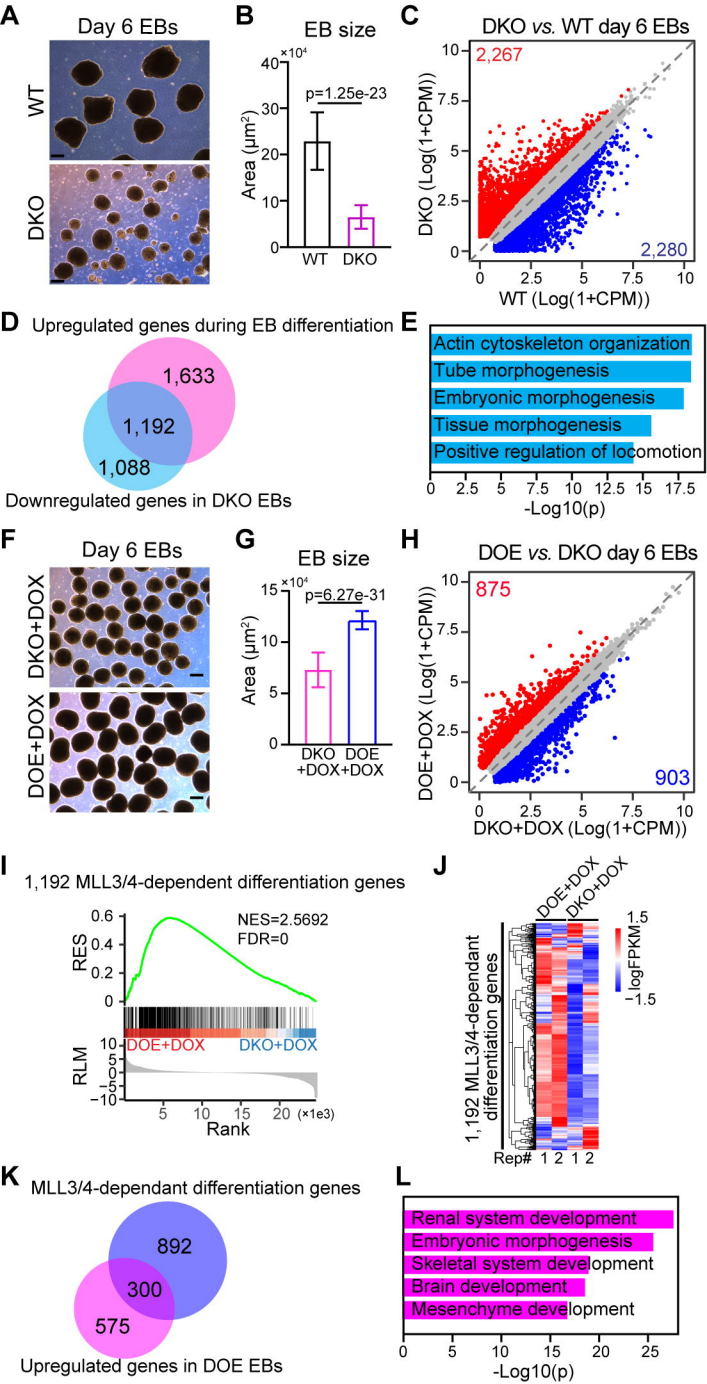
A
Day 6 EBs
WT
DKO
B
EB size
×10⁴
Area (μm²)
p=1.25e-23
WT
DKO
C
DKO vs. WT day 6 EBs
2,267
2,280
DKO (Log(1+CPM))
WT (Log(1+CPM))
D
Upregulated genes during EB differentiation
1,633
1,192
1,088
Downregulated genes in DKO EBs
E
Actin cytoskeleton organization
Tube morphogenesis
Embryonic morphogenesis
Tissue morphogenesis
Positive regulation of locomotion
-Log10(p)
F
Day 6 EBs
DKO+DOX
DOE+DOX
G
EB size
×10⁴
Area (μm²)
p=6.27e-31
DKO +DOX
DOE +DOX
H
DOE vs. DKO day 6 EBs
875
903
DOE+DOX (Log(1+CPM))
DKO+DOX (Log(1+CPM))
I
1,192 MLL3/4-dependent differentiation genes
NES=2.5692
FDR=0
RES
RLM
DOE+DOX
DKO+DOX
Rank
(×1e3)
J
DOE+DOX
DKO+DOX
1,192 MLL3/4-dependant differentiation genes
-logFPKM
Rep# 1 2 1 2
K
MLL3/4-dependant differentiation genes
892
300
575
Upregulated genes in DOE EBs
L
Renal system development
Embryonic morphogenesis
Skeletal system development
Brain development
Mesenchyme development
-Log10(p)